



EUROPEAN
COMMISSION

European
Research Area

Long-term Performance of Engineered Barrier Systems

PEBS

Contract (grant agreement) number: *FP7 249681*

DELIVERABLE (D-N°:D2.3-6-2)

**FORMATION OF IRON OXIDE AND OXYHYDROXIDES UNDER
DIFFERENT ENVIRONMENTAL CONDITIONS**

Iron/bentonite interaction

Author(s):

Elena Torres, María Jesús Turrero, Alicia Escribano and Pedro Luis Martín

Date of issue of this report: **14/03/14**

Start date of project: **01/03/10**

Duration : **48** Month

Revised	Approved

Project co-funded by the European Commission under the Seventh Euratom Framework Programme for Nuclear Research & Training Activities (2007-2011)		



Table of contents

1. Introduction	2
1.1. Evolution of environmental conditions during the performance of a DGR	4
1.1.1 Emplacement of the waste packages and dry-out period	5
1.1.2 Unsaturated conditions of the bentonite barrier	6
1.1.3. Anaerobic saturated conditions	9
2 Description of the experimental framework	10
3 Materials and methods	11
3.1 Description of the experimental set-up	11
3.1.1. General experimental set-up	11
3.2 Characterization techniques	16
3.2.1 THM analysis	16
3.2.2 Geochemical characterization	16
3.2.3 Characterization of corrosion products	16
4 Results	17
4.1 Water content and dry density measures	17
4.2 Geochemical characterization of the bentonite blocks from the dismantled medium cells	19
4.2.1 Chloride	19
4.2.2 Sulfate	20
4.2.3 Soluble cations	21
4.2.4 Exchangeable cations	22
4.3 Characterization of corrosion products	25
4.3.1 Small-cell tests	25
4.3.2 Medium cells. Corrosion tests under unsaturated conditions	29

5	DISCUSSION.....	36
6.	Conclusions	37
7.	References	38

Figures

Figure 1. Corrosion layer growth rate as a function of the relative humidity. Tests conducted at 343K and 20% O ₂ -80%N ₂ atmosphere [16].	7
Figure 2. Weight gain of salt covered A516 carbon steel versus time as a function of relative humidity. Specimens had nominally 5 mg of deposited NaCl. Also included for comparison in the plot for a clean specimen exposed to 90% RH.[23].	8
Figure 3. Duration of the tests carried out in the framework of NF-Pro and PEBS projects and their correspondence with a representative time scale in the performance of the repository.	11
Figure 4. a) Diagram of the experimental set-up for medium cells; the experimental design for small cells is identical, but with different dimensions; b) Diagram showing the configuration of the samples inside the small and medium cells and the location of the sensors in the medium cells. (Not to scale)	14
Figure 5. Picture of the small (left) and medium (right) cells used in this work.	15
Figure 6. Evolution of relative humidity in the bentonite blocks from the medium cells dismantled: FB1 (6 months), FB2 (15 months) and FB3 (52 months).	18
Figure 7. Distribution of soluble chloride found in the three medium-cell tests dismantled.	20
Figure 8. Distribution of soluble sulfate found in the three medium-cell tests dismantled.	21
Figure 9. Distribution of soluble cations along the bentonite blocks found in the three medium-cell tests dismantled.	23
Figure 10. Distribution of exchangeable cations along the bentonite blocks found in the three medium-cell tests dismantled.	24
Figure 11. Scheme of the sampling performed in the iron powder from the dismantled medium cells.	30
Figure 12. Photograph taken after the dismantling of the 6-month medium cell: (left) bentonite surface; (right) iron powder.	31
Figure 13. Photograph taken after the dismantling of the 15-month medium cell: (left) bentonite surface; (right) corroded iron powder.	31
Figure 14. TEM characterization of the corrosion products found in the 15-month test: a) TEM image of the hematite nanocrystals found in the pink suspension together with the corresponding SAED pattern and EDS analysis; b) TEM image of the phases found	

in the brown suspension: b1) non-identified Cl-rich phase and b2) poorly-crystalline hematite together with their corresponding SAED patterns and EDS analysis..... 33

Figure 15. Photograph taken after the dismantling of the 52-month medium cell: (left) bentonite surface; (right) corroded iron powder..... 34

Figure 16. Scheme of the corrosion products found in the lab cell tests (Fe powder) as a function of the duration of the test..... 35

Tables

Table I. Evolution of environmental conditions in a Deep Geological Repository characterized in terms of the stages of saturation [8].	4
Table II.- Main chemical species (ppm) in the BO-ADUS groundwater (Grimsel Test Site) used to hydrate FB cells.	15
Table III. Water content and dry density values measured in medium cells dismantled after 6 and 15 months of operation.	18
Table IV. Water content and dry density values measured in the medium cell dismantled after 54 months.	19
Table V. Corrosion products found in the small cells where hydration was not applied	25
Table VI. Evolution of corrosion products found in the dismantled medium cell as a function of test duration.	29
Table VII. Summary of results obtained from the characterization of corrosion products found in the dismantled medium cells.	35

EXECUTIVE SUMMARY

This deliverable summarizes the results obtained in the corrosion tests carried out in the framework of NF-PRO and PEBS projects at CIEMAT.

The aim of the report is to summarize available information for the modelling of corrosion processes observed in the tests assembled during NF-Pro to study the alteration processes at the Fe/bentonite interface [1-4].

The structure of this document is divided into a review of the existing literature, a brief description of the materials and the cylindrical cells used in the tests and the summary of the results obtained from the small and medium cells already dismantled.

1. INTRODUCTION

Carbon steel is one of the candidate materials for the waste package in the Spanish High-Level Waste (HLW) Disposal Project. These waste packages will be emplaced in a granitic host formation. As buffer material, a Na-Ca-Mg bentonite (FEBEX bentonite) has been chosen by the Spanish radioactive waste management agency (ENRESA). The clay barrier will be made of blocks of powder FEBEX bentonite with its hygroscopic water content ($\approx 14\%$) compacted to a dry density of 1.65 g/cm^3 .

Waste packages will be exposed to different environmental conditions since their emplacement until long-term steady-state conditions are achieved after tens of thousands of years. Corrosion behaviour of the carbon steel canisters will depend strongly on the evolution of the mechanical, hydraulic, physical and chemical parameters of the clay barrier along the lifetime of the repository [5].

The thermal output of each waste package is expected to be 1.2 kW at the time of emplacement. Due to the low thermal conductivity of unsaturated FEBEX bentonite ($0.39 \text{ Wm}^{-1}\text{K}^{-1}$), maximum temperature at the canisters surfaces is expected to be $100 \text{ }^\circ\text{C}$ and is predicted to be reached ten years after their emplacement. Water content redistribution along the bentonite is assumed to occur shortly after the emplacement of the waste packages. High temperature will provoke the dry-out of the bentonite blocks in the proximity of the canisters. Water vapour will diffuse through unsaturated bentonite until reaching the coldest zones of the barrier and condensate in them. Different matrix suction along the clay barrier (higher in the hot areas than in the colder ones) will favour the formation of convection cells, what will lead to the progressive salt enrichment of bentonite pore water in the vicinity of the canisters, especially during post-closure and transient state.

Temperature at the canister surface will decrease due to radioactive decay. Lower temperatures and the increasing moisture content will favour the increase of thermal conductivity ($1.4 \text{ Wm}^{-1}\text{K}^{-1}$ for saturated FEBEX bentonite). Calculations [6] show that temperature at the metallic surface will decrease to around $50 \text{ }^\circ\text{C}$ after 5000 years. Full saturation of the bentonite barrier will lead to the homogenization of the chemical composition of the pore water along the clay barrier.

Moisture conditions at the canister surface will determine the mechanism and extension of the corrosion process. During the gradual saturation of the near-field, deliquescence of salts (i.e. halite, gypsum) and other impurities will favour the initialization of localized corrosion phenomena.

Saline fronts are expected to be formed during the saturation of the clay barrier. Chloride and sulfate will move by advective transport towards the metallic container due to the hydraulic and thermal gradients that will be established along the bentonite barrier.

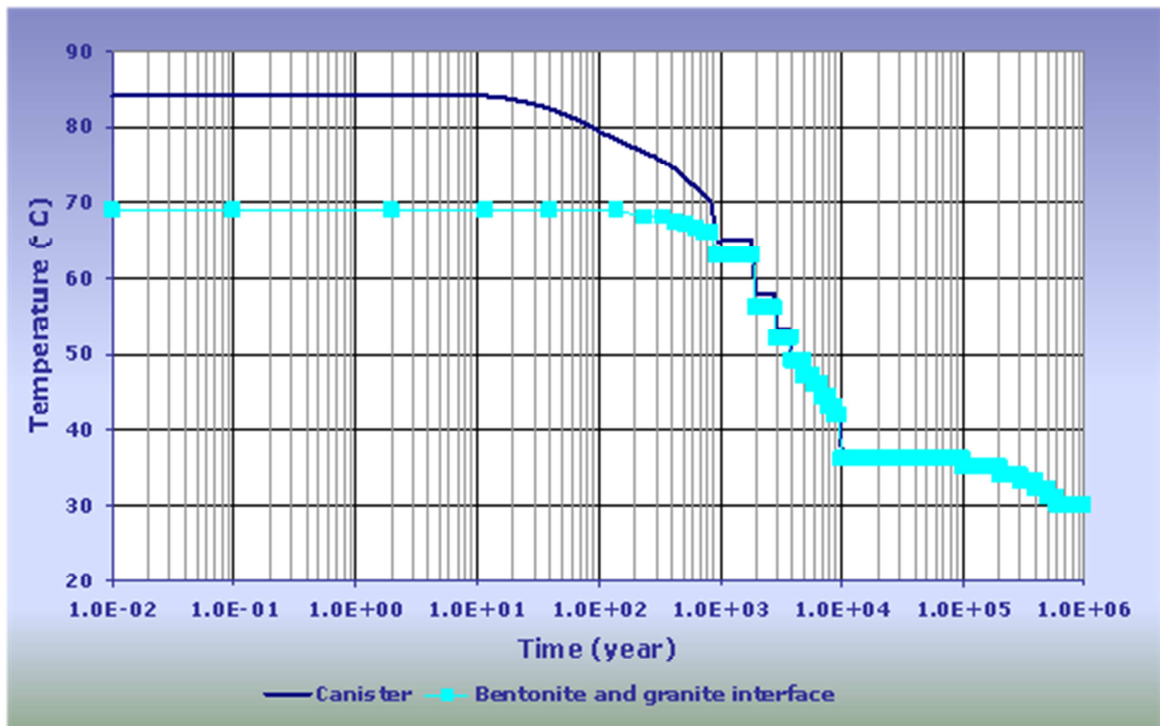


Figure 1. Time evolution of temperatures at the canister and bentonite-granite interface [7].

Table I summarizes the environmental conditions expected during the lifetime of a DGR as a function of the degree of saturation of the bentonite barrier.

Table I. Evolution of environmental conditions in a Deep Geological Repository characterized in terms of the stages of saturation [8].

Dry-out phase	Transition phase	Saturated phase
Redistribution of initial moisture content	Gradual saturation of bentonite	Complete saturation of bentonite
Poor thermal conduction	Improving thermal conduction	Good thermal conduction
No swelling of sealing materials	Development swelling pressure	Swelling pressure fully developed
Dissolution and reprecipitation of minerals	Dissolution of minerals	Gradual equilibration of pore water with groundwater
No deliquescence	Deliquescence of precipitated salts	Corrosion in fully saturated bentonite
No corrosion	Corrosion due to formation of thin surface water film	H ₂ generation once O ₂ depleted
No gas generation	H ₂ generation possible once O ₂ depleted	O ₂ completely consumed
No O ₂ consumption	O ₂ consumption	Onset of anoxic conditions
No microbial activity	No microbial activity in highly compacted bentonite	No microbial activity in highly compacted bentonite
Possible tunnel convergente	Tunnel convergence	

1.1. Evolution of environmental conditions during the performance of a DGR

A DGR may be subjected to 3 or 4 different hydrological regimes, depending on the authors' criteria, over its lifetime:

1.1.1 Emplacement of the waste packages and dry-out period

Due to decay heat, desiccation of bentonite blocks and precipitation of hygroscopic salts are likely to occur after the emplacement of the waste packages. Canisters will be in contact with hot moist air. However, there is insufficient water adsorbed on the canister surface to support generalized aqueous corrosion processes.

Surface contaminants on the metal surface will favour the absorption of moisture coming from desorption of hygroscopic water in the bentonite blocks closer to the canisters. Regarding the distribution of the surface impurities and the oxygen content of the disposal gallery (initially equal to the atmospheric content - 20% in volume), some degree of localised attack can be expected.

After the emplacement of the canisters, water is driven away from the repository drifts. A hot dry atmosphere will prevail in the vicinity of the containers. Low permeability of unsaturated FEBEX bentonite, together with the thermal output of spent fuel will determine the evolution of moisture conditions at the canister surface.

During the dry-out period, RH values at the steel/bentonite interface are expected to be very low, insufficient to allow electrochemical corrosion to continue. In this period, it is possible that corrosion products may transform into more stable iron phases due to high temperature and low RH values achieved at the interface. Although, it is expected that dry conditions protect the surface of the metal canister from corrosion, and oxidation of steel at RH lower than Critical Relative Humidity (CRH) is possible (Critical Relative Humidity is the threshold value at which water vapour can condensate and form aqueous films on the metallic surface).

Oxidation of steel in dry atmospheres is one potential degradation mode for iron-based materials at moderately elevated temperatures expected at the container surface (50-200 °C). The effect of water vapour on the corrosion products formed at temperatures close to the boiling point of water is not well documented [9, 10]. However, according to the physically-based model calculations, dry oxidation is not expected to significantly degrade the performance of thick corrosion allowance barriers made of low-carbon steel. Stahl and McCoy [11] presented the following empirical equation (Eq. 1) to predict the penetration rate of a carbon steel barrier due to high temperature oxidation:

$$P = 1.787 \times 10^5 t^{0.33} \exp(6780/T) \quad \text{Eq. 1}$$

where: p is the penetration depth in μm , t is the exposure time in years, and T is temperature in Kelvins. Equation 1 predicts a negligible penetration of less than 0.02 μm in 1000 years at the boiling point of water [12].

Oxidation of iron and low-carbon steel produces multi-layered scales due to the variable oxidation state iron. In order of proximity to the metal surface these are: FeO (wüstite), Fe₃O₄ (magnetite) and Fe₂O₃ (hematite). However, at temperatures below 570 °C, FeO

is thermodynamically unstable, so only Fe_3O_4 and Fe_2O_3 form [13]. At these moderately elevated temperatures, the Fe_3O_4 layer is found to be much thicker than the Fe_2O_3 layer, at least for scales up to about 20 μm thick [14].

Corrosion rates under such conditions are expected to be less than 0.2-0.3 μm [15, 16]. Corrosion films formed on low-carbon steel consist basically of nanometric layers of anhydrous iron oxides, such as hematite ($\alpha\text{-Fe}_2\text{O}_3$) and/or magnetite (Fe_3O_4).

During this period, some of the O_2 entrapped in the bentonite will be consumed by corrosion of steel rock support materials and by microbial processes in regions of the repository that are wetter and cooler than at the surface of the canister. As noted above, corrosion of the rock support materials could consume all of the trapped O_2 within a period of a few decades [5].

1.1.2 Unsaturated conditions of the bentonite barrier

After temperatures in the drift drop below the boiling point of water, hot humid conditions will return. The surface of the canister will start to wet due to deliquescence of salt crystals, condensation in the pores of the pre-formed oxide films and other surface discontinuities. During this period, localized attacks of certain importance are likely to occur until achieving anaerobic saturated conditions.

Corrosion under unsaturated conditions - Absence of deposited salts

In the absence of salt deposits, the rate of corrosion below 50% RH can be neglected. The critical value of 60% for the relative humidity has often been reported for iron [17], to be the border between the domain of chemical reactions ($\text{RH} < 60\%$) and the domain of electrochemical reactions ($\text{RH} > 60\%$) (Figure 1).

Ben Lagha [17] reported a drastic mass increase at RH values above 70%, though at the lower value of 50%, the amount of water adsorbed on the surface seems sufficient to induce electrochemical reactions. According to Dante & Kelly [18], an initial adsorption of 10 to 20 monolayers of water, is the minimum amount of water necessary for electrochemical reactions.

The rate of growth of the corrosion products film reaches its maximum at $\text{RH}\% > 70\%$. The porosity of the corrosion products formed during this period is determined by the transport of the reacting species. At RH values below 70%, the joint action of an impervious surface layer made of magnetite and maghemite, and an insufficient water amount, explains that electrochemical reactions are hindered. At higher RH values, the corrosion layer is first expected to be very porous, allowing the formation of hydrated oxides (lepidocrocite, goethite) at the oxide/water interface. These hydrated species progressively plug up the pores [19], leading to the slowing down of the rate of oxide. A trend of slowing down is also observed at 80% RH.

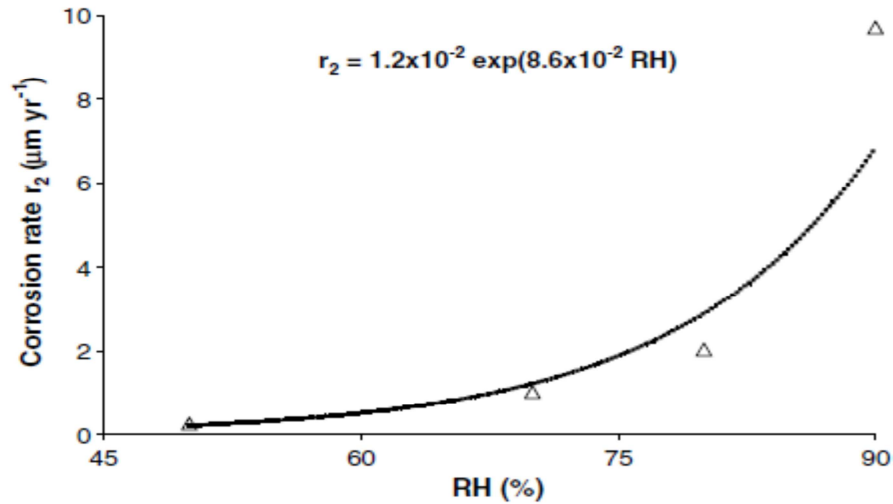


Fig. 2(b). Corrosion layer growth rate during period 2 as a function of the value of relative humidity.

Figure 1. Corrosion layer growth rate as a function of the relative humidity. Tests conducted at 343K and 20% O₂-80%N₂ atmosphere [16].

Analysis of the corrosion layers formed at the different RH values shows that magnetite Fe₃O₄ and maghemite γ -Fe₂O₃ are present at all of the tested RH values, whereas hydroxides (goethite α -FeOOH and lepidocrocite γ -FeOOH) were only detected for RH values equal or above 70%. Magnetite and maghemite were localized near the metallic surface, whereas hydroxides were mainly present in the upper part of the rust layer.

Enhanced corrosion under unsaturated conditions – Hygroscopic conditions

Hygroscopic salts are known to significantly enhance the corrosion of mild steel at relative humidity below 100% [20]. The aqueous salt solutions formed enable aqueous film electrochemical corrosion of the steel to occur. The severity of the corrosion is dependent on the particular salt and the relative humidity (Figure 2). It has been noted that, in general, the severity of attack of steel as a function of relative humidity increases significantly at RH values equal to or greater than the equilibrium relative humidity of the saturated salt solution. Bulk aqueous salt solutions will form at the equilibrium relative humidity.

However, there is a noted increase in the corrosion of steel even at relative humidity values below the equilibrium value when compared to the corrosion in the absence of the deposited salt [20]. In terms of the cations, salts of sodium (Na) and potassium (K) have higher equilibrium RH's (less hygroscopic) than those of calcium (Ca) and magnesium (Mg).

In terms of the anions, sulfates and nitrates have higher equilibrium RH's (less hygroscopic) than those of chlorides. For some salts, such as, sodium chloride (NaCl), there is little change in the equilibrium RH as a function of the temperature, probably because the solubility of NaCl does not change much with temperature.

At RH values less than the equilibrium value, bulk aqueous salt solutions will not form. At RH values greater than the equilibrium value, more dilute aqueous solutions will form. The amount of water that is taken up by hygroscopic salts, such as, NaCl, have been previously determined as a function of relative humidity [21]. At 100 °C and 74% RH (the equilibrium RH), there are about 2.6 mg of water taken up per mg of NaCl. At 100 °C and 85% RH, there are about 4.4 mg of water taken up by per mg of NaCl. At 100 °C and 91% RH, there are about 7 mg of water taken up by per mg of NaCl.

The corrosive action of deposited salts, such as NaCl and Na₂SO₄, on carbon steel is well documented [20]. Under normal atmospheric conditions, it is recognized that the effectiveness of sustaining the corrosion processes decreases with time for a given amount of initially deposited salt. It is documented that chloride ions are incorporated into the iron oxide akaganite under marine conditions [22]. Sulfate has been identified within solid corrosion products. The mineral jarosite, NaFe₃(OH)₆(SO₄)₂ or KFe₃(OH)₆(SO₄)₂, has been suggested as an example of a potential iron and sulfate containing compound that could form during corrosion [22]. Graedel and Frankelthal [5] have discussed the topic of mineral formation during corrosion in some detail.

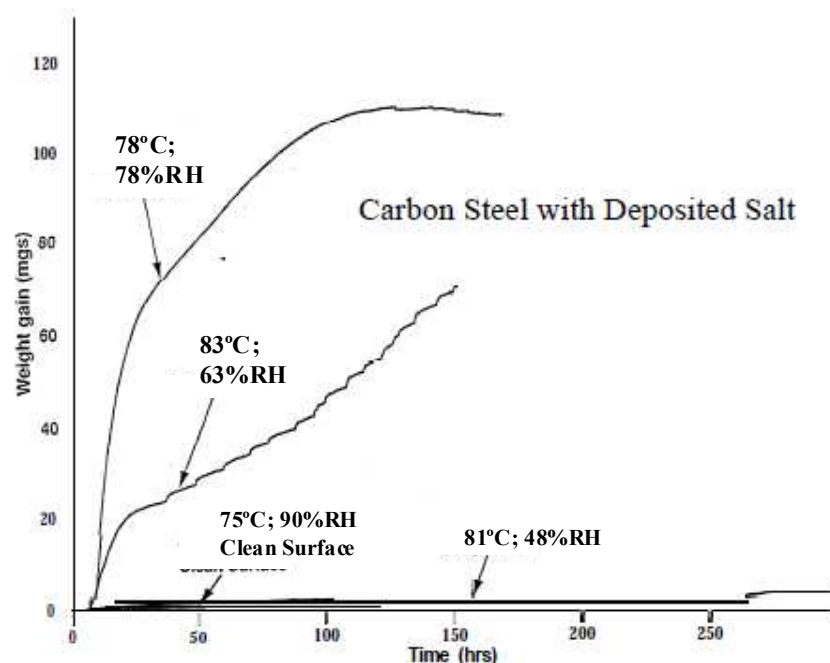


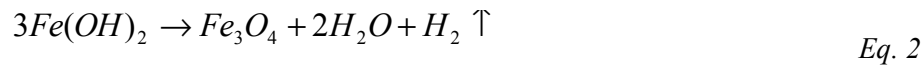
Figure 2. Weight gain of salt covered A516 carbon steel versus time as a function of relative humidity. Specimens had nominally 5 mg of deposited NaCl. Also included for comparison in the plot for a clean specimen exposed to 90% RH. [23]

1.1.3. Anaerobic saturated conditions

After the saturation of the bentonite barrier, the chemical composition of bentonite porewater will homogenize due to diffusion. Saline fronts generated in previous stages due to the thermal gradients along the bentonite barrier will disappear.

After the oxygen has been exhausted, the nature of the corrosion processes will change and the formation of hydrogen gas will begin to dominate [24]. The amount of available oxygen, the availability of water, the hydration conditions, and the reaction kinetics will determine which solid phase will prevail [25].

When anoxic conditions are attained, steel will continue to corrode by direct reaction with water by the following reaction [25-29]:



giving an overall reaction:



Although Fe_3O_4 is the thermodynamically favored end product, $Fe(OH)_2$ may actually dominate at temperatures below 60 °C, since the conversion reaction (eq. 2) may be inhibited or at least delayed [30].

Smart et al. [31] have, however, observed passivation due to magnetite formation at temperatures as low as 30 °C. If the corrosion potential exceeds the equilibrium potential of magnetite formation, an impervious oxide film is formed on the metal surface as a protective coating against further corrosion. This effect is called passivation. In the passive state, metal dissolution is determined by the balance between slow passive film dissolution on the outer surface and film formation at the metal-film interface. These conditions occur for iron under anaerobic conditions in alkaline environments [25].

From eq.1, 2 and 3, it is evident that the anaerobic corrosion of the metallic overpack could result in the formation of substantial hydrogen concentrations in the underground repository during the anoxic period. If the production rate of hydrogen is higher than its migration rate through the backfill, the hydrogen activity could exceed the hydrostatic pressure in the repository, resulting in gas bubble formation. Such an occurrence could have a detrimental effect on nuclide transport in the near-field, and may even cause cracking of a concrete engineered barrier [26].

A build-up of hydrogen pressure within the repository can lead to a reduced driving force for the corrosion reactions, thereby inhibiting the formation of $Fe(OH)_2$ or Fe_3O_4 .

From thermodynamic calculations (free energy changes), it is known that the overpressure required to suppress the production of ferrous hydroxide and magnetite is 140 and 80 MPa respectively. Therefore, in view of the limited hydrostatic pressure available in the repository, the hydrogen overpressure cannot suppress the corrosion reactions completely [32].

2 DESCRIPTION OF THE EXPERIMENTAL FRAMEWORK

The work presented in this report was performed in the framework of NF-PRO and PEBS projects to investigate the influence of FEBEX bentonite geochemistry in the corrosion of iron powder and carbon steel and the possible alteration processes undergone by bentonite due to corrosion.

As the experimental results were planned to be extrapolated to real conditions, the most realist approach possible was applied. Same materials and operational parameters as the ones considered for the Spanish concept were used.

Experiments were performed in hermetic cells that allow the application of thermal and hydraulic gradients similar to the ones expected during the repository operation. In order to simulate the interaction between the bentonite barrier and the carbon steel canisters, compacted bentonite blocks in contact with iron powder or carbon steel plates were used.

Due to the limited time scale of the lab programme if compared with the lifetime of the repository, corrosion processes had to be accelerated (Figure 3). In most of the tests, carbon steel plates were substituted by Fe powder in order to avoid the kinetic restrictions and to enhance the corrosion process, and therefore, the effect of dissolved Fe on compacted bentonite.

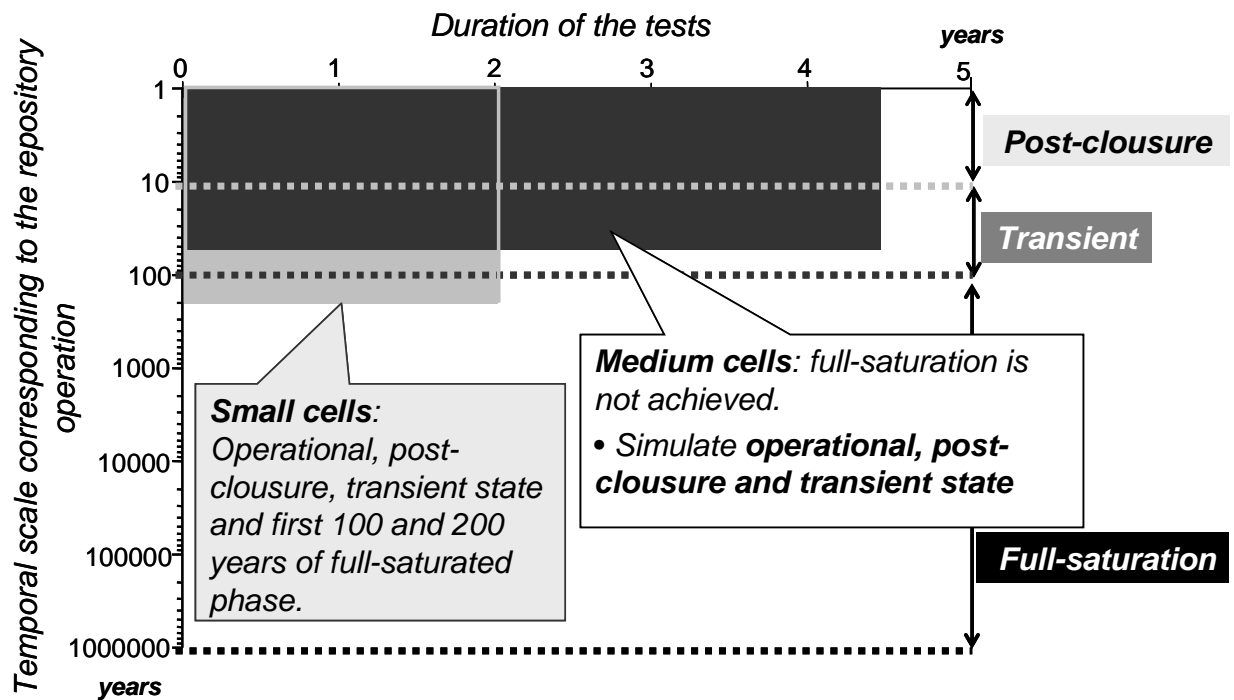


Figure 3. Duration of the tests carried out in the framework of NF-Pro and PEBS projects and their correspondence with a representative time scale in the performance of the repository.

3 MATERIALS AND METHODS

3.1 Description of the experimental set-up

The tests were performed in cylindrical cells especially designed to simulate the environmental conditions expected during the operation of the repository. These cells were especially designed for the experiments in the previous project NF-PRO [33] and are scaled similarly to a real repository.

In order to tackle the up-scaling effect on the processes observed in the tests, two different cell sizes were used, small and medium cells, though they share the same characteristics related to design and materials.

3.1.1. General experimental set-up

The medium cells own an internal diameter of 7 cm and an inner length of 10 cm. In the small cells dimensions are 5 cm diameter and 2.5 cm length. Both are made of Teflon[®] to prevent as much as possible lateral heat conduction. The upper closing of the cells is made by means of a stainless steel plug. Inside this plug there is a deposit in which water circulate at a constant temperature of 30 °C. The bottom part of the cell is a plane stainless steel heater set at 100 °C. In this way, a constant gradient between top and bottom of the sample is imposed. Hydration is made through the upper plug of the cell

with water stored in a stainless steel pressurized deposit. The plug has concentric grooves in the plane in contact with the filter that allow a better distribution of the water. The deposit is periodically weighed to check the water intake. A porous stainless-steel filter with pore size of 0.45 μm is placed between the plug and the sample. A schematic diagram of the set-up and a picture of the cells are shown in Figure 4.

Blocks of FEBEX bentonite were compacted with its hygroscopic water content (14%) at a nominal dry density of 1.65 g/cm^3 and placed inside the cells.

In order to get a conservative approach to the unsaturated and oxidizing conditions expected during the post-closure stage, iron powder was used. The aims of using iron powder instead of bulk carbon steel were, on one hand, maximizing corrosion rate by the increase of the reactive surface and on the other hand, decreasing the O_2 fugacity because of the consumption of residual oxygen during the corrosion process. Goodfellow iron powder with a maximum particle size of 60 μm and a purity higher than 99% (Typical Analysis: Si <1400, C <200, HLoss <3000, P <150, S <150, in ppm) was used to contact with bentonite. Iron powder was chosen in order to enhance corrosion phenomena, as the high specific surface of the iron particles help to overcome kinetic constrains.

Once the assemblage mounted the temperature of the heater was initially set to 100 $^\circ\text{C}$. The upper cooling was set at room temperature (25 $^\circ\text{C}$). Finally, hydration from the deposit started immediately after assembling the whole system. The deposit was initially pressurized with nitrogen at 5 bars. The water injected to hydrate the iron/bentonite cells was granite water (Table II) collected every year in the Grimsel Test Site from the BO-ADUS borehole. This borehole is close to the in situ FEBEX experiment, a full-scale experiment to study the processes influencing clay barrier evolution in a granite formation [34]. The water is alkaline (pH 9.7), reduced, Na-Ca- HCO_3^- type. The reducing character of water was preserved during hydration. The injection deposit was periodically weighed, and this allowed checking the water intake.

Special features of the small cells

In order to identify the sequence of corrosion products formation, four identical tests were conducted in the small cells and were dismantled sequentially at different times: 21 days, 2, 4 and 6 months. In these tests, no hydration was applied. So, unsaturated conditions prevailed during all the experiments.

Apart from the described experiments, a TStE355 carbon steel plate was tested in a small cell to confirm results obtained in the tests where Fe powder was used. Steel plates were prepared according to metallographic protocols based on manual grinding on silicon carbide (SiC) papers (#320, #500, #1000). To study corrosion of steel under unsaturated conditions, no hydration was applied.

Special features of the medium cells

Medium cells were instrumented with capacitive-type sensors placed inside the clay at two different levels (Figure 4). The transmitters used are Sensirion HMP237, which include a relative humidity (RH) sensor and a temperature sensing element. The RH values are converted to suction values through Kelvin's law.

A uniaxial pressure of 43 MPa was applied to manufacture 86.8-mm long bentonite blocks for the medium cells. At the bottom of the cell, in contact with the heater, 143.4 g of Fe powder were placed, giving rise to an iron layer thickness of 13.0 mm (Figure 4). On top of this, the bentonite block was inserted and a porous filter over it.

Six cells (FB1 to FB6) were mounted at a time, starting on May 2006, thinking in a sequential dismantling to have a view of the succession of processes. All of them were ensambled and run in the same way, except for Cell FB6, in which no hydration takes place. Two of them were dismantled during the NF_PRO project, after 174 (Cell FB1) and 480 (Cell FB2). Another cell was dismantled after 4 years and 6 months of operation (Cell FB3 y FB4).

When each reactor was closed, residual oxygen was trapped inside. Environmental conditions evolved from oxidant to reducing conditions. Similar evolution is expected after the closure of the repository, during transient state. Usually, lab tests devoted to corrosion are conducted under oxidant or under reducing conditions, but few regard the progressive oxygen depletion inside the repository.

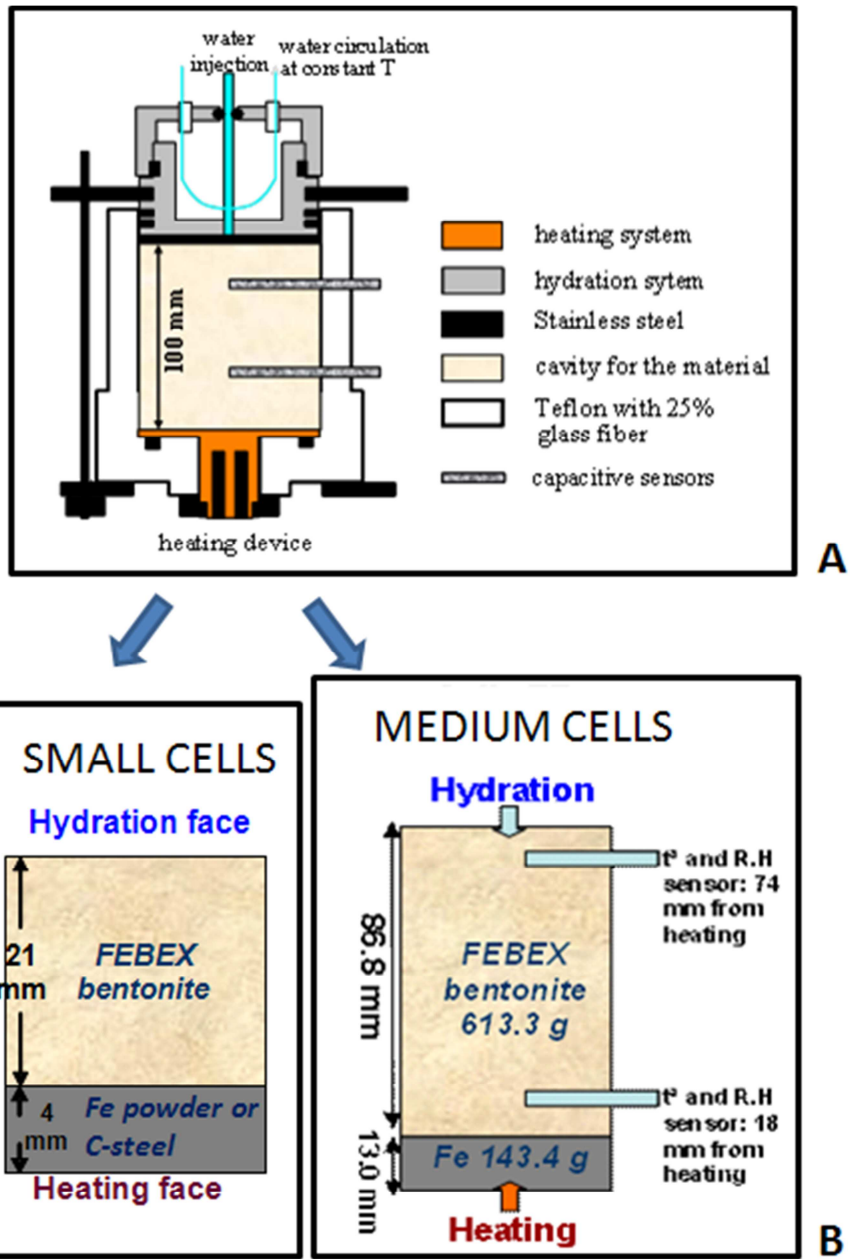


Figure 4. a) Diagram of the experimental set-up for medium cells; the experimental design for small cells is identical, but with different dimensions; b) Diagram showing the configuration of the samples inside the small and medium cells and the location of the sensors in the medium cells. (Not to scale)



Figure 5. Picture of the small (left) and medium (right) cells used in this work.

Table II.- Main chemical species (ppm) in the BO-ADUS groundwater (Grimsel Test Site) used to hydrate FB cells.

Chemical species	Concentration (ppm)
Na ⁺	8.60 ±0.06
Ca ²⁺	7.35±0.24
Mg ²⁺	0.40 ±0.01
K ⁺	0.88 ±0.10
SO ₄ ²⁻	5.90 ±0.22
Cl ⁻	0.82 ±0.04
F ⁻	4.13 ±0.10
Alk (HCO ₃ ⁻)	24.25 ±0.37
SiO ₂	11.40 ±0.08
pH	9.7 ±0.13
Eh	-153 mV

3.2 Characterization techniques

3.2.1 THM analysis

At the end of the tests, the cells were dismantled and the clay blocks extracted. Once extracted, the bentonite columns were sawed in cylindrical sections used for the different determinations.

The gravimetric water content (w), defined as the ratio between the mass of water and the mass of dry solid, was determined by oven drying at 110 °C for 48 hours. Dry density (ρ_d) is defined as the ratio between the mass of the dry sample and the volume occupied by it prior to drying. The volume of the specimens was determined by immersing them in a recipient containing mercury and by weighing the mercury displaced, as established in UNE Standard 7045 “Determination of soil porosity”.

3.2.2 Geochemical characterization

Each of the bentonite zones was used to analyze soluble elements in aqueous extract solutions. Bentonite samples were dried overnight in an oven at 60 °C. They were ground and placed in contact with deionised and degassed water at a solid to liquid ration of 1:8 (5 of clay in 40 mL of water), shaken end-over-end and allowed to react for 24 hours. Separation was made by centrifugation (30 minutes at 12500 rpm) and the supernatant was filtered by a 0.45- μ m pore size filter.

Cations in supernatants were analysed by Inductive Coupled Plasma - Optical Emission Spectrometry (ICP-OES) in a Spectro ARCOS spectrometer after acidification of the samples to pH<2 with HNO₃ (8 ml/l). Anions were analysed using ion chromatography (Dionex DX-4500i). Total alkalinity of the samples (expressed as HCO₃⁻ concentration) was determined by potentiometric titration using a Titroprocessor Metrohm 716 DMS. The analyses were made by means of a specific Dynamic Equivalence point Titration (DET) method. Additional measures of soluble salts were performed at the interface.

To determine the exchangeable cations of the samples, a CsNO₃ solution was used to displace the exchangeable cations. Bentonite samples were equilibrated with CsNO₃ 0.5 N at pH 8.2 at a solid to liquid ratio of 0.25 kg/L. After phase separation by centrifugation, the supernatant solutions were filtered by 0.45 μ m and the concentration of the major cations was analysed by ICP-OES.

3.2.3 Characterization of corrosion products

FTIR spectra of corrosion products and bentonite samples were obtained in the middle-IR region (4000-400 cm⁻¹) with a Nicolet 6700 with a DTGS KBr detector (resolution 4 cm⁻¹, 40 scans) on KBr-pressed discs in transmission mode.

X-ray diffraction patterns were recorded on random powder samples of bulk bentonite and iron oxides. Samples were analysed with a PHILIPS X'PERT MPD diffractometer, using a Cu anticatode and a graphite monocromator at 45 kV and 50 mA. The scan rate used was 1° 2 θ /min.

SEM-EDS characterization of the samples was done with a SEM JEOL JM-6400 microscope coupled to a dispersive X-ray energy spectrometer X LINK LZ_5. Iron oxide samples were metallised with gold, whereas in the bentonite samples a graphite coating was deposited on them.

For TEM examination, a JEOL 2000FX operating at 200 kV acceleration voltage (3.4 Å point- to-point resolution) was coupled to an OXFORD ISIS X-ray energy dispersive spectrometer giving a resolution of 136 eV at 5.39 KeV.

The sample preparation for the TEM observation of the corrosion products consisted on a suspension of the corroded iron powder in ethanol. After separation by sedimentation, the suspension was dropped on a carbon coated copper grid.

Room temperature Mössbauer spectra were obtained in transmission mode using a constant acceleration drive and triangular reference signal. A ⁵⁷Co/Rh source with initial activity of 25 mCi was used. The spectra were fitted using a program called DIST3E .

4 RESULTS

This section is intended to compile the results obtained after the dismantling of both, the small and the medium-sized cells. Medium-cell tests attempt to simulate unsaturated conditions during transient state, whereas the small ones would reproduce the environmental conditions generated after the full saturation of bentonite.

4.1 Water content and dry density measures

The water contents near the heater were in all the cases lower than initial and not very different among the three cells, what would indicate that desiccation (i.e. water vapour movement) was quick and persistent and that the liquid water did not reach the bottom of the bentonite column after 1593 days (Figure 6).

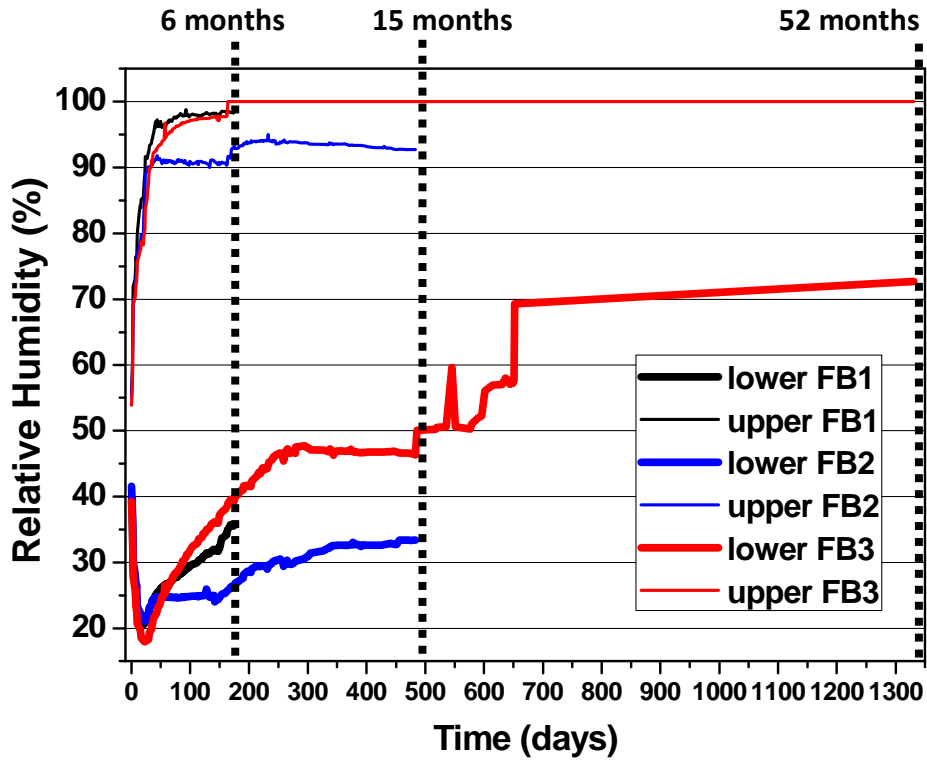


Figure 6. Evolution of relative humidity in the bentonite blocks from the medium cells dismantled: FB1 (6 months), FB2 (15 months) and FB3 (52 months).

Water content and dry density values measured in the medium cells already dismantled are displayed in Table III and Table IV.

Table III. Water content and dry density values measured in medium cells dismantled after 6 and 15 months of operation.

	6 months			15 months		
	Section I (hydration)	Section II (intermed)	Section III (heater)	Section I (hydration)	Section II (intermed)	Section III (heater)
Distance from hydration (mm)	14	42	71	14	42	71
Water content(w%)	32.6	---	10.5%	25.9	17.6	9.6
Dry density (g/cm ³)	1.41	---	1.69	1.53	1.56	1.76

Table IV. Water content and dry density values measured in the medium cell dismantled after 54 months.

Section	Section I	Section II	Section III	Section IV	Section V
Distance from hydration (mm)	12	32	47	57	75
Water content (w%)	32,9	31,5	28,6	22,2	11,8
Dry density (g/cm ³)	1.44	1.46	1.50	1.53	1.70

4.2 Geochemical characterization of the bentonite blocks from the dismantled medium cells

4.2.1 Chloride

High temperature causes the desiccation of the bentonite block and induces the precipitation of salts at the interface (chlorides and carbonates mainly). Salt precipitation may play a relevant role in the performance of the carbon steel canister in the repository. Chloride precipitates are well-known for being hygroscopic. This fact could lead to the formation of very concentrated brines on the surface of the canister, what could favour localized corrosion.

The most relevant transport processes occurring in the cell may be deduced from the behaviour of chloride. The Cl⁻ distribution is closely related to the water advection, with the formation of saline fronts moving towards the heat focus. Chloride is easily dissolved when less saline water enters the column and is transported as the hydration front moves to the unsaturated areas, as previously Cuevas et al. [35]. The advance of Cl⁻ depends on the duration of the experiment. In the FB1 (174 days) experiment, the maximum chloride content was localized in the intermediate zone. As the hydration front advanced, as in FB2 (480 days), chloride was concentrated at the heating zone and the interface (hottest zone). According to the chemical analysis made on FB3 (1593 days), still unsaturated, Cl⁻ concentration is also higher at the interface. Data obtained from the chemical analysis indicate that advection prevails over diffusion as mechanism for salt movement (Figure 7).

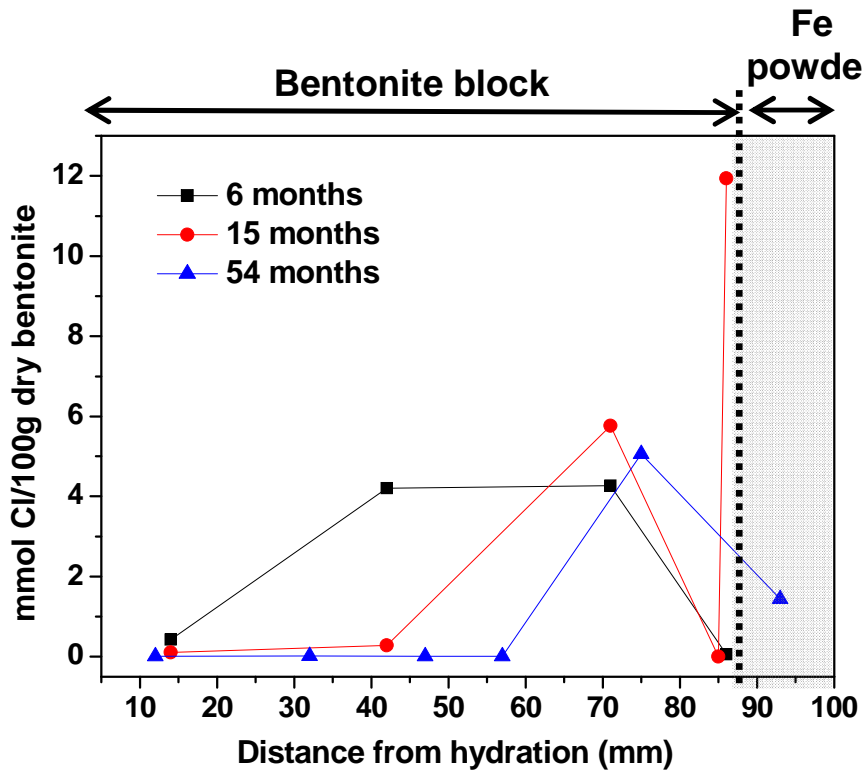


Figure 7. Distribution of soluble chloride found in the three medium-cell tests dismantled.

The increase of salinity in the hottest parts of bentonite is possibly caused by the formation of small convection cells generated due to the thermal gradient. At the iron/bentonite interface, water absorbed in bentonite evaporates and moves towards the coldest areas, where it condensates. Liquid water moves again towards the heater. During this movement, the most soluble minerals are dissolved. The hydration front transports salts and saline fronts are generated along the bentonite block. The mobility of these fronts depends on each element. Cuevas et al. [36] however, proposed that the driving force for salt transport would be the increase of salt concentration on the mesopore “external” water with respect to the “surface-influenced” (anion exclusion) micropore water. The preservation of primitive interfaces between the stacks of montmorillonite lamellae and the macrograins (i.e. quartz) upon saturation can be a proof of the maintenance of preferential pathways for salt migration.

4.2.2 Sulfate

Sulfate concentration patterns are more complex, as this specie is affected by dissolution/precipitation and ion exchange (Figure 8).

The SO_4^{2-} content increases with time due to the solubilization of gypsum. Sulfate is leached from the saturated sections, as well as chloride. However, the kinetics is slower than that of the Cl^- anions. The mobility of sulfate is hindered if compared to Cl^- , because of its retention on clay surfaces mainly by electrostatic repulsion (higher ionic charge/radii ration than Cl^-) [37]. Leaching of sulfate could occur because of the formation of neutral ionic pairs ($\text{Mg}^{2+}/\text{SO}_4^{2-}$, $\text{Ca}^{2+}/\text{SO}_4^{2-}$) which can move easily between the charged clay surfaces. This could enhance the movement of the SO_4^{2-} [35].

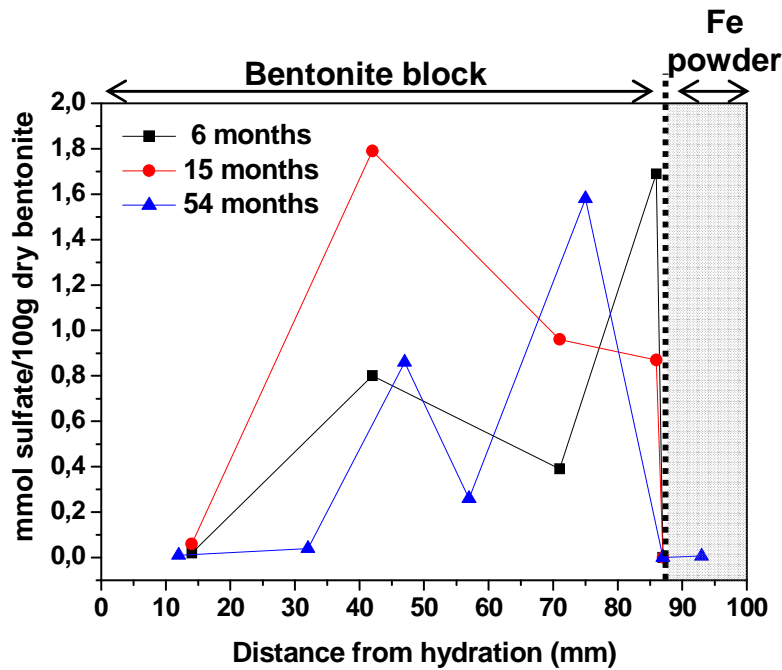


Figure 8. Distribution of soluble sulfate found in the three medium-cell tests dismantled.

4.2.3 Soluble cations

The main counterion that followed chloride in all the tests is sodium, decreasing close to the hydration source and increasing towards hotter zones (Figure 9). However, sodium concentration is not only controlled by advective transport but also by cation exchange reactions.

There is an overall increase of magnesium, calcium and potassium along the bentonite block. As in the case of sodium, they are moving towards the heater and concentrating at the interface. In the case of the 52-month tests, appreciable amounts of soluble Ca and Mg were detected not only at bentonite near the interface, but in Fe powder.

4.2.4 Exchangeable cations

The distribution of exchangeable cations varies along the bentonite blocks (Figure 10). Some authors have reported the change in the selectivity coefficients as a function of temperature. According to them, the selectivity coefficient of magnesium increases with temperature, whereas, in the case of sodium, it decreases at higher temperature. That fact could explain the increase of magnesium in the exchange complex in zones closer to the heater.

Magnesium and sodium seem to follow complementary trends along the bentonite column. Exchangeable sodium increases close to the hydration surface and drops near the interface, whereas magnesium decreases in saturated zones and increases near the heater. Sodium exchanges by magnesium in the saturated areas. Magnesium is released from the interlayers to pore water in the coolest zone and is transported to the hottest zone [38]. Near the heater, magnesium released in saturated areas enters the exchange complex. Magnesium–complexes seem to be more stable at high temperatures than the complexes formed by the rest of the exchangeable cations.

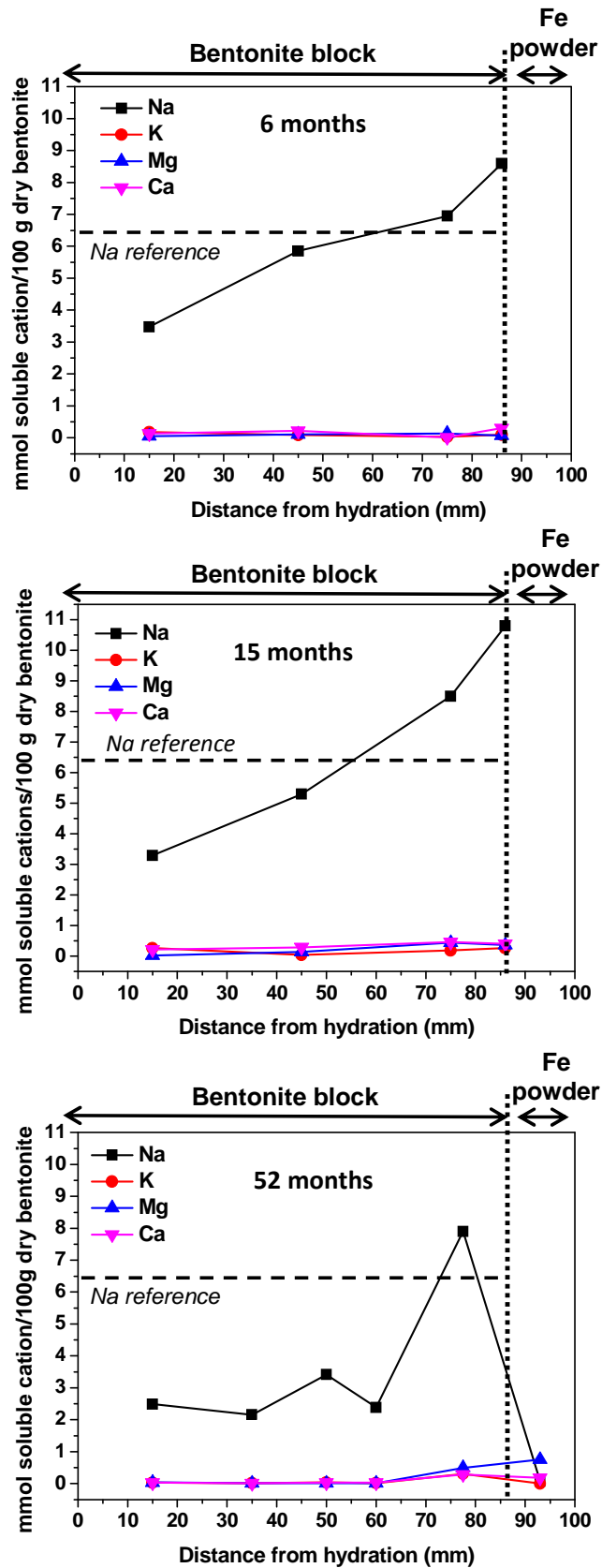


Figure 9. Distribution of soluble cations along the bentonite blocks found in the three medium-cell tests dismantled.

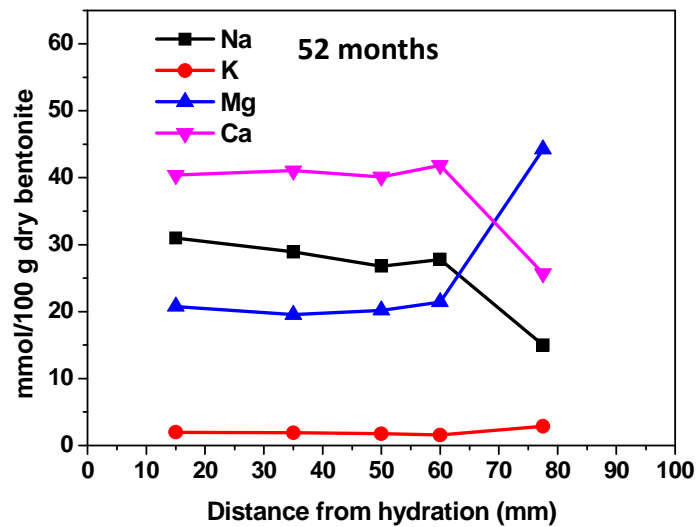
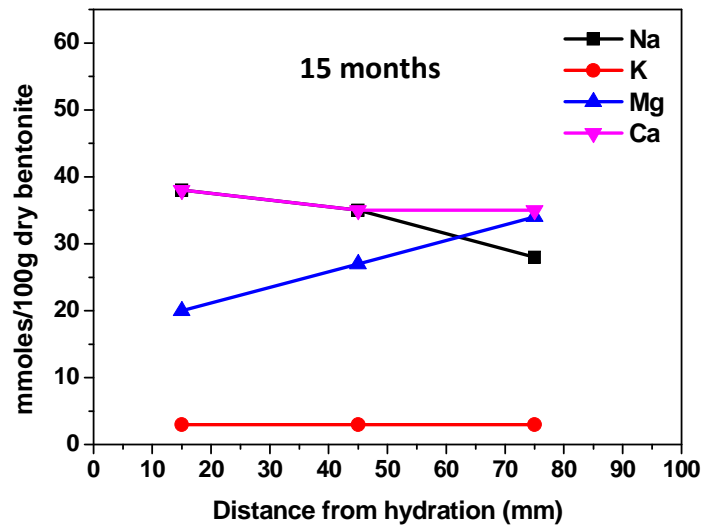
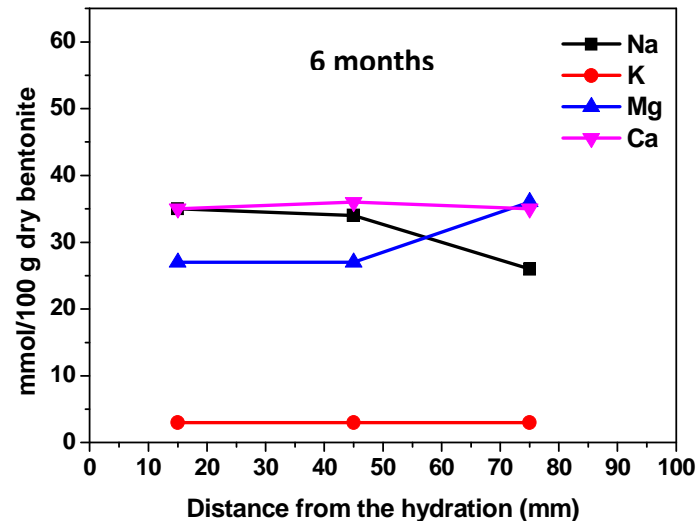


Figure 10. Distribution of exchangeable cations along the bentonite blocks found in the three medium-cell tests dismantled.

4.3 Characterization of corrosion products

4.3.1 Small-cell tests

Fe powder

In order to identify the sequence of corrosion products formation, four identical tests were conducted in the small cells and dismantled sequentially at different times: 21 days, 2, 4 and 6 months. In these tests, no hydration was applied. So, unsaturated conditions prevailed during all the experiments. These experiments were designed to simulate the conditions generated in the clay barrier during the post-closure and dry-out period of the DGR.

Main components in the corrosion products found in the four tests were iron oxyhydroxides, either lepidocrocite or goethite (Table V). It seems that lepidocrocite is the prevalent oxyhydroxide at shorter times, whereas goethite appears at longer ones. According to results obtained, it seems that there is a sequence in the order of formation of the corrosion products. $\text{Fe}(\text{OH})_3$ acts as precursor of iron oxyhydroxides.

Lepidocrocite is the first oxyhydroxide to be formed. However, it is a metastable compound that evolves to more stable iron oxides. Goethite is thermodynamically favored when relative humidity is lower than 50% [39]. The sequence of corrosion product formation identified in these tests is in good agreement with thermodynamics. Corrosion kinetics has little impact on the nature of corrosion products when iron powder is used due to the great reactive surface of the powder.

Table V. Corrosion products found in the small cells where hydration was not applied

Time	Corrosion Products
3 weeks	$\text{Fe}(\text{OH})_3$, Lepidocrocite ($\gamma\text{-FeOOH}$)
2 months	Lepidocrocite ($\gamma\text{-FeOOH}$)
4 months	Lepidocrocite ($\gamma\text{-FeOOH}$), Goethite ($\alpha\text{-FeOOH}$)
6 months	Lepidocrocite ($\gamma\text{-FeOOH}$), Goethite ($\alpha\text{-FeOOH}$)

C-steel plates

In the steel plate, localized corrosion phenomena were observed on the surface several pits were formed during the 22 months the test was running.



Figure 11. Photograph of the pitted surface of the steel plate after 22-month exposure to unsaturated compacted bentonite

Formation of pits is usually related to the presence of contaminants on the metal surface. Initialization of pits usually occurs in areas of the metal surface where high chloride contents are detected (salt islands). However, in this case, no passive layer was observed on the metal surface. The tested steel plate preserved its metallic luster. Surface of the steel plate remained mostly uncorroded. A nanometric magnetite layer was grown in few dispersed areas but did not exhibit any protective role.

The big-sized pits were possibly initiated during the first months of the test, when RH was higher due to the evaporation of adsorbed water in bentonite. An electrochemical mechanism is necessary for the formation of the pits, so moisture was required. Moisture was available at the interface in the first moments of the test, so the nucleation of the pits seems to be previous to the formation of magnetite. In the case of magnetite, no high RH values were required.

In any case, the lack of hydration and the high temperature at the interface will preserve the metal surface from corrosion. However, desiccation of bentonite induced the accumulation of hygroscopic salts on the carbon steel surface. Evaporation of bentonite adsorbed water and the deposition of bentonite dust can lead to the formation of deposits on the steel surface.

These hygroscopic salts could sorb moisture from the atmosphere and form brine solutions, which potentially could cause aqueous corrosion of the metals. In addition, the corrosion process could form products that in combination with these salts have an even lower deliquescence point that could result in aqueous corrosion at lower relative humidity.

In the case of the tests performed, the precipitation of solid particles of chloride is likely to enable the initialization of the pits. EDS confirmed the existence of high chlorine contents. However, no chlorine was found in the mouth of the pit or in the non-corroded surface, so most of it is expected to be accumulated at the bottom of the pit.

Once the pit is initiated, it grows autocatalytically. Ferrous ions are released by the interaction of the electrolyte (H₂O) with the metal surface. The ferrous ions then attract the negatively charged chloride ions into the initiation site and hydrolysis occurs by the reaction (Eq. 4):



There is a local decreasing in pH resulting from the liberation of hydrochloric acid, and this further accelerates anodic dissolution. At the bottom of the pits, Raman microspectroscopy confirmed the formation of Cl-rich phases (akaganeite). However in the mouth of the pits, hematite and maghemite were mainly formed. Lepidocrocite was also detected in the outer part of the pits. In pitting corrosion, iron oxyhydroxides (both goethite and lepidocrocite) are usually formed. As it has been observed in the Fe powder tests, iron oxyhydroxides transform into hematite and maghemite by dehydration.

Magnetite found in the metal surface could be formed in dry atmospheres, by the interaction of the gas or the vapor generated inside the cell.

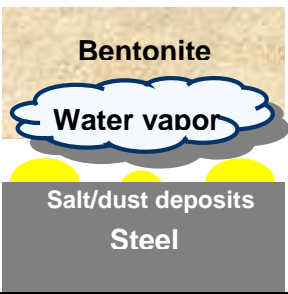
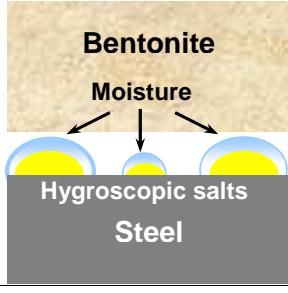
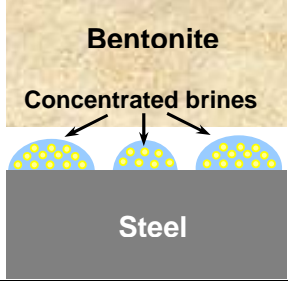
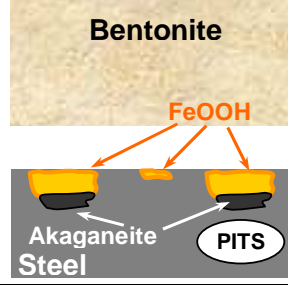
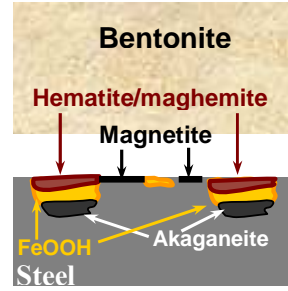
Corrosion under unsaturated conditions		
Step 1	Evaporation of adsorbed water 	<ul style="list-style-type: none"> Evaporation of adsorbed water in bentonite Precipitation of salts (chloride, carbonates) Deposition of dust from desiccation of bentonite
Step 2	Sorption of moisture 	<ul style="list-style-type: none"> Sorption of moisture by hygroscopic salts
Step 3	Formation of brines 	<ul style="list-style-type: none"> Salts dissolve and form wet droplets Formation of concentrated brines of the metal surface
Step 4	Electrochemical mechanism 	<ul style="list-style-type: none"> Electrochemical corrosion (with participation of residual oxygen trapped): $2Fe(s) + 4H^+(aq) + 4Cl^-(aq) + O_2(g) \rightarrow 2Fe^{2+}(aq) + 4Cl^-(aq) + 2H_2O$ $2Fe^{2+}(aq) + 4Cl^-(aq) + 3H_2O + \frac{1}{2}O_2 \rightarrow 2FeOOH(s) + 4H^+(aq) + 4Cl^-(aq)$ Nucleation and growth of pits on the steel surface: $Fe^{2+} + 2H_2O + 2Cl^- \rightarrow Fe(OH)_2 + 2HCl$ Formation of FeOOH (goethite and lepidocrocite) and akaganeite [$\sim FeO_{0.833}(OH)_{1.167}Cl_{0.167}$]
Step 5	Dry atmosphere at the interface 	<ul style="list-style-type: none"> High temperature and lack of hydration: low relative humidity at the interface Formation of a thin layer of magnetite: “dry-corrosion” mechanism: $3Fe + 4H_2O \rightarrow Fe_3O_4 + 4H_2 \uparrow$ Dehydration of FeOOH: $2(\alpha, \gamma) - FeOOH \xrightarrow{\Delta} (\alpha, \gamma) - Fe_2O_3 + H_2O$

Figure 12. Scheme of the processes occurred at the steel/bentonite interface during corrosion under unsaturated conditions.

4.3.2 Medium cells. Corrosion tests under unsaturated conditions

Sequential dismantling of the cells allowed studying the influence of time and relative humidity on the nature of the corrosion products.

According to the data obtained from the three tests dismantled, it could be inferred that the nature of corrosion products will depend, mainly, on RH values, temperature and oxygen concentration. RH has a great importance in the nucleation and growth of the iron oxide. Higher RH values would allow a slow nucleation and growth of the crystal, what would favor a more crystalline phase. At this point, it should be noticed the importance of the precipitation of hygroscopic salts, and especially chloride, on the surface of the iron powder. Chloride precipitates enable the formation of thin aqueous films at low relative humidity. Usually, corrosion products formed by this mechanism are amorphous or poorly crystalline.

The use of Fe powder in these tests enhances corrosion due to its high reactive surface but introduces new variables. The heterogeneity of Fe powder can favor the formation of preferential pathways for the movement of vapour, so there will be particles that will be more exposed than others to the oxidizing agent. This could explain the coexistence of corroded and non-corroded particles in the tests. In the case of carbon steel plates, this phenomenon is not relevant as the exposed metal surface of the bulk material is homogeneous if compared with Fe powder.

Table VI shows three photographs taken after the dismantling of each medium cell. The sequence of formation of corrosion products begins with the precipitation of $\text{Fe}(\text{OH})_3$ and lepidocrocite followed by goethite. As relative humidity decreases near the interface, the formation of anhydrous oxides is more likely to occur (hematite, maghemite). As saturation of the bentonite block progresses and residual oxygen is depleted, magnetite prevails.

Table VI. Evolution of corrosion products found in the dismantled medium cell as a function of test duration



In the three dismantled cells, the analysis of the iron powder collected at different distances from the Fe/bentonite interface showed that Fe powder was scarcely corroded. The scheme of the sampling performed in the iron powder from the dismantled cells is shown in Figure 11. Most corroded iron was mainly found at the Fe/bentonite interface. Chlorine was detected in the corrosion products but not in the non-corroded particles. From this, it could be inferred that precipitated chloride in iron powder might have a relevant role in the initialization of corrosion. Precipitated particles of chloride at the interface might induce localized corrosion phenomena, as chloride is well-known to be a hygroscopic salt and to be able to absorb environmental moisture. Absorption of moisture by salt precipitates leads to the formation of concentrated brines on the metal surface and precipitation of Cl-rich phases, such as akaganeite, is likely to occur.

Due to the importance of chloride for the initialization of corrosion, special attention has been paid to its distribution at the Fe/bentonite interface. Chloride distribution in the Fe powder was not homogeneous but localized in small areas spread all over the interface. Preferential pathways could explain localized precipitation of chloride. Retractive cracks formed in the bentonite blocks in zones close to the interface could favour the formation of preferential pathways. These preferential pathways will be possibly responsible for the transport and accumulation of salts in localised areas at the Fe/bentonite interface.

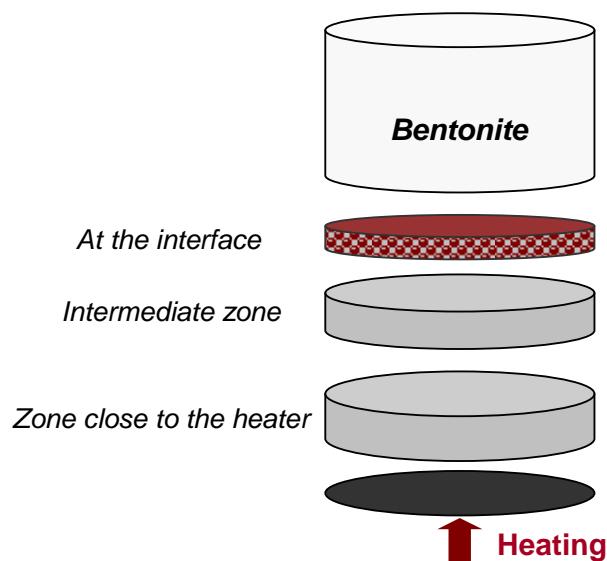


Figure 11. Scheme of the sampling performed in the iron powder from the dismantled medium cells.

6-month test

In the 6-month test, goethite was formed at the interface, on the surface of the bentonite block. High chlorine contents achieved in localized areas at the interface could induce the formation of Cl-substituted goethite (Figure 12).

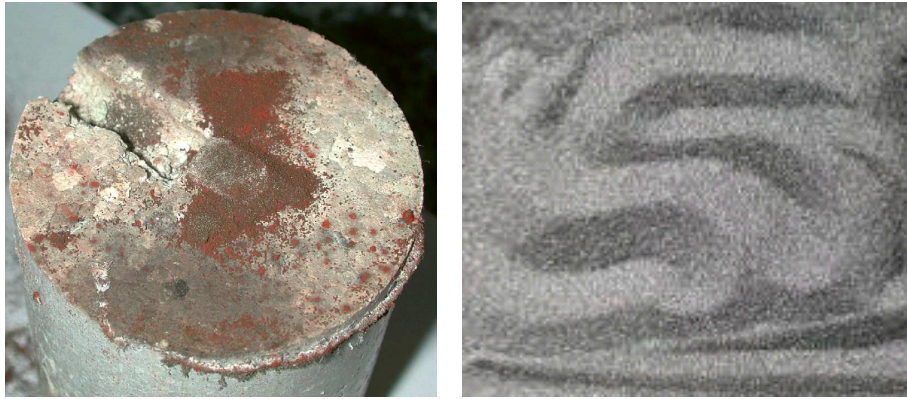


Figure 12. Photograph taken after the dismantling of the 6-month medium cell: (left) bentonite surface; (right) iron powder.

15-month test

In the 15-month test, hematite was identified, both at the interface and in the Fe powder (Figure 13). Again, chlorine was detected in the corrosion products (Figure 14).



Figure 13. Photograph taken after the dismantling of the 15-month medium cell: (left) bentonite surface; (right) corroded iron powder.

Characterization of corrosion products was difficult due to the slight corrosion undergone by Fe powder. For that reason, TEM and SAED techniques were used for the identification of the corrosion products found in Fe powder not in direct contact with bentonite.

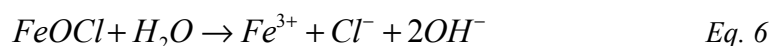
As corroded Fe powder, in this case, exhibited two different colors, purple and brown, different corrosion products were expected in each sample. In order to confirm it, Fe

samples were suspended in ethanol. After sonication, the solution was decanted. Corrosion products suspended in ethanol were deposited on a carbon-coated copper grid for TEM observation. Figure 14 shows three TEM micrographs and their corresponding SAED patterns recorded for samples collected from the 15-month tests.

TEM confirmed the existence of iron oxide nanoparticles in both suspensions. In the case of the pink suspension, well-developed nanocrystals were found. In the brown suspension, however, nanoparticles exhibited rough surfaces and poorly crystalline structures. EDS analysis of corrosion products detected, in most cases, traces of chlorine. Precipitation of chlorine was not homogeneous. Average value calculated for the studied samples was 0.6%at., however in some crystals, it reached up to 7%at.

SAED spot patterns obtained for the purple corrosion products were consistent with haematite. EDS analysis of diffracted crystals confirmed the presence of chlorine. As no Cl-rich phases were identified, it seems that chlorine was not incorporated into the crystalline lattice, but deposited on the surface of crystals.

Characterization of iron oxide nanoparticles found in the brown suspension revealed the co-existence of several corrosion products. SAED patterns showed that corrosion products exhibited a poorly-crystalline structure. Spot patterns were consistent with the superposition of several individual particles in different crystallographic orientations. EDS analysis detected high contents of chlorine, but no Cl-rich phases could be identified in the SAED diffraction patterns. These SAED patterns were not consistent with the lattice parameters of any iron oxide reference pattern, maybe because the studied oxide was a metastable phase. Parameters obtained, however, were similar to the ones tabulated for FeOCl. FeOCl is an intermediate compound that acts as a catalyst in the corrosion of steel. Reactions in which it is involved are shown in equations 5 to 7:



being the overall reaction:



Chloride, in this case, could introduce into the structure of the iron oxides. The decomposition of these Cl-rich phases would lead to the formation of HCl and the acidification of the media. Apart from this metastable compound, poorly-crystallised haematite was identified.

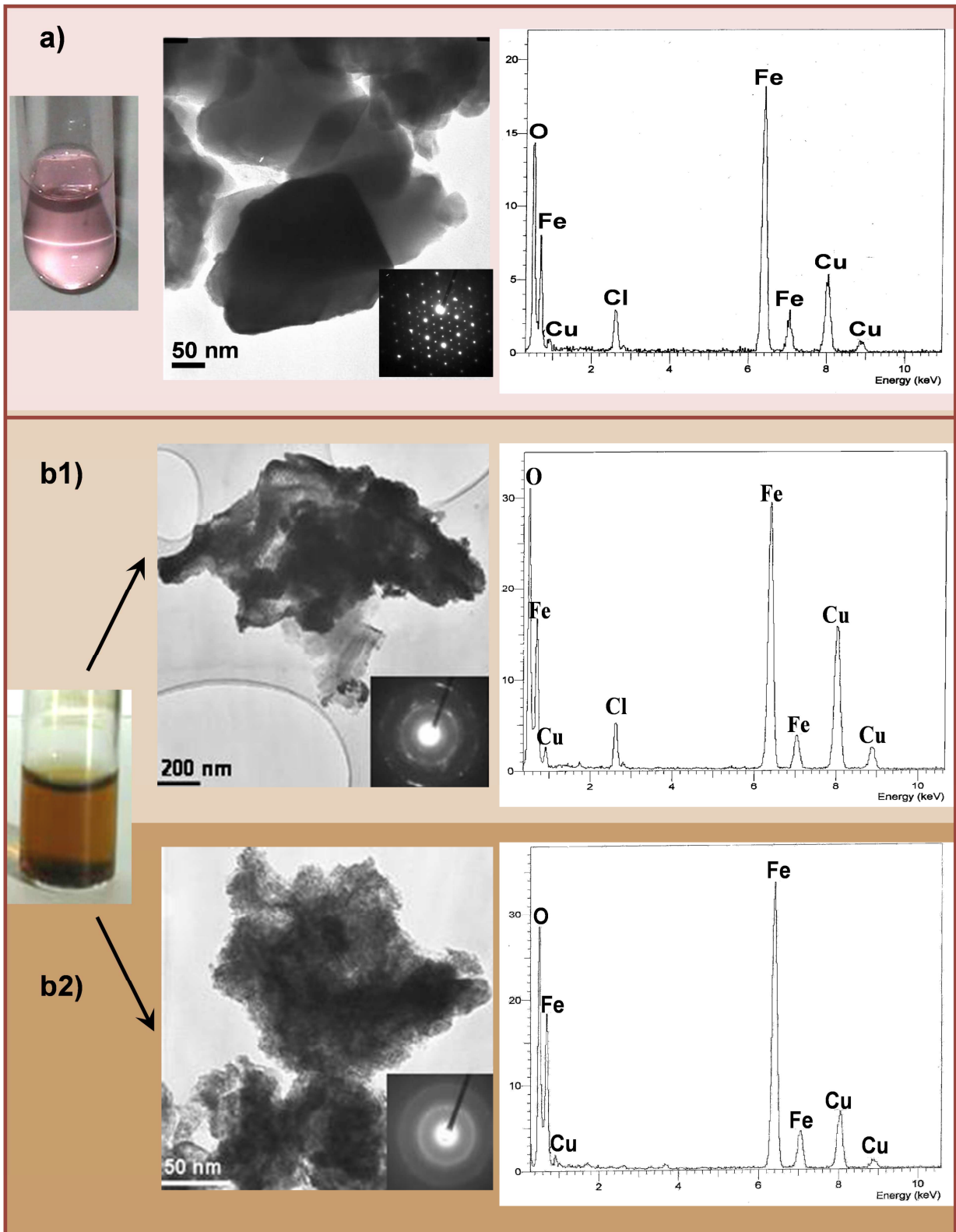


Figure 14. TEM characterization of the corrosion products found in the 15-month test: a) TEM image of the hematite nanocrystals found in the pink suspension together with the corresponding SAED pattern and EDS analysis; b) TEM image of the phases found in the brown suspension: b1) non-identified Cl-rich phase and b2) poorly-crystalline hematite together with their corresponding SAED patterns and EDS analysis.

52-month test

As observed in the 6 and 15-month tests, extension of corrosion processes was limited. Average thickness of the iron oxide layer around Fe powder particles was few tens of nanometers.

In the 52-month test, additionally to the corrosion products found in the previously dismantled tests, a new blue compound was found in the fraction of Fe powder close to the heater. This fraction remained uncorroded in the 6 and 15-month tests..

Iron powder was sampled and analyzed based on differences of color observed after the dismantling: red at the interface, purple in the intermediate zone and blue in the contact with the heater (Figure 15).

The red fraction, in contact with the bentonite block, consisted basically of iron oxyhydroxides, such as lepidocrocite, goethite and akaganeite. At the intermediate fraction, the purple one, haematite was the prevalent corrosion product. FTIR analyses conducted on the purple/blue fraction confirmed the existence of magnetite (Fe_3O_4) and ferrous hydroxides. The formation of Fe(II)-phases indicates that reducing or nearly-reducing conditions have been achieved inside the cell.

EDS identified traces of chlorine in Fe particles collected at different distances from the interface. This fact was confirmed by the soluble extracts analyses performed in Fe powder samples collected. High soluble chloride contents were measured in the Fe samples, which could be related to the role of Fe powder as a sump for chloride.



Figure 15. Photograph taken after the dismantling of the 52-month medium cell: (left) bentonite surface; (right) corroded iron powder.

Table VII summarizes the results obtained from the characterization of corrosion products found in the dismantled medium cells.

Table VII. Summary of results obtained from the characterization of corrosion products found in the dismantled medium cells.




	Fe powder		
	6 months	15 months	52 months
			
Date of dismantling	February 2007	November 2008	December 2010
Location of corrosion products	At the interface	At the interface + small fraction of Fe powder	All Fe powder corroded
Corrosion products			
At the interface	Goethite	Goethite	Goethite
Intermediate fraction	×	Hematite	Hematite
Close to the heater	×	×	Magnetite + hydrated ferrous oxides

Figure 16 tries to represent schematically the sequence of formation of the different iron oxides found and their correspondence with the duration of the tests and size of the cells used.

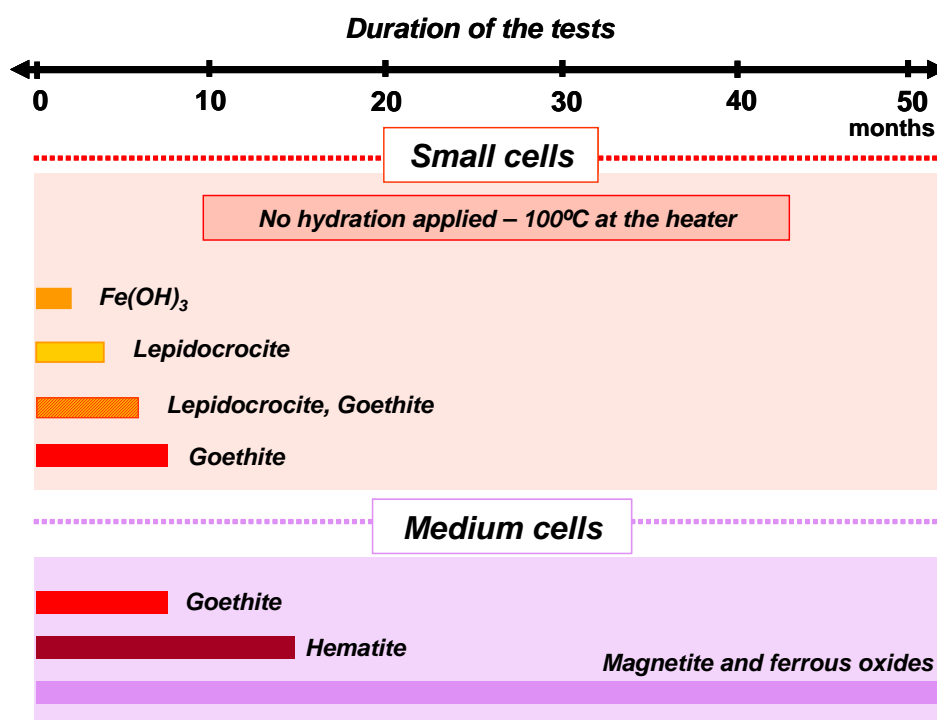


Figure 16. Scheme of the corrosion products found in the lab cell tests (Fe powder) as a function of the duration of the test.

5 DISCUSSION

Both series of tests were designed in order to reproduce the evolution of environmental conditions after the emplacement of waste packages. Thus, initial aerobic conditions evolve to a reducing environment inside the reactors. The increase of RH near the Fe powder due to the bentonite re-saturation and the depletion of trapped oxygen favoured the formation of mixed Fe(II)/Fe(III) phases.

In all cases, corrosion was negligible. When Fe powder was used, in the first two tests dismantled (6 and 15 months), corrosion was scarce and localized, especially in Cl-rich areas in the vicinity of the bentonite surface. In the 52-month test, corrosion became more uniform.

The thickness of oxide layers coating the Fe particles ranged from less than 1 micron in the contact with bentonite to few tens of nanometers in the contact with the heater, despite high reactivity of particulate iron.

Chloride seems to play a relevant role on the initialization of corrosion. In the absence of salt deposits, the rate of corrosion below 50% RH is usually neglected. The critical value of 60% for the relative humidity has often been reported for iron [17], to be the border between the domain of chemical reactions ($RH < 60\%$) and the domain of electrochemical reactions ($RH > 60\%$). According to Dante & Kelly [18], an initial adsorption of 10 to 20 monolayers of water, is the minimum amount of water necessary for electrochemical reactions. Water content measured in the proximity of the Fe/bentonite interface was in all cases below 60%. However, intrinsic properties of Fe powder, such as moisture sorption isotherm, and water activity at the interface may displace this threshold to lower values of Relative Humidity.

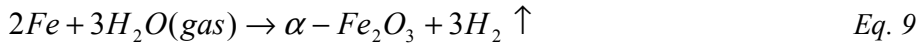
The sequential dismantling of the tests allowed studying the sequence of formation of corrosion products: Fe(III) oxides at shorter times and mixed Fe(II)/Fe(III) phases at longer durations. Goethite and hematite were the main corrosion products identified in the 6-month and 15-month tests, respectively. In the 52-month test, mixed Fe(II)/Fe(III) hydroxides were the prevailing corrosion products.

Goethite was the prevailing phase during the first 6 months. Goethite is thermodynamically more stable than lepidocrocite at low RH. Due to the slow re-saturation of the bentonite block, desiccation leads to its transformation into hematite according to the following reaction (Eq. 8):

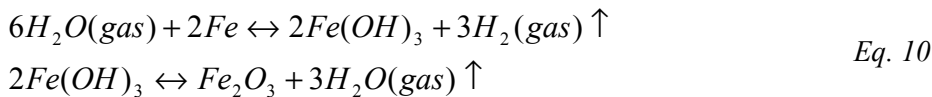


Although hematite was the prevailing iron oxide in the 15-month test, poorly-crystalline maghemite was formed as well. Iron powder in close contact with the heater or close to it remained mainly non-corroded as RH was kept at low values ($>20\%$).

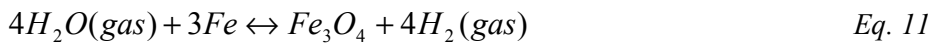
In the 15-month test, formation of hematite at the interface could occur as a consequence of dehydration of goethite. However, this mechanism would not explain the formation of hematite and maghemite found in iron powder at longer distances from the interface. Thus, corrosion of Fe powder via dry oxidation is likely to occur. Due to high temperature and water vapor, iron powder could corrode according to the following reactions (Eq. 9 and Eq. 10):



or



As residual oxygen is depleted, magnetite is likely to appear. Magnetite formation can be described via Eq. 11. This mechanism seems to be in good agreement with the results obtained in the carbon steel plate tested in unsaturated conditions. In this case, the metallic surface exhibited a discontinuous nanometric scale composed of magnetite.



6. CONCLUSIONS

Conclusions inferred from both series of tests are, basically, that:

- A chloride front is generated along the bentonite block and moves towards the heater.
- Chloride at the Fe/bentonite interface is not homogeneously distributed.
- Pits are initiated in the first moments of the tests, and salt and dust deposits could play a relevant role in the initialization of corrosion
- Fe powder act as a sump for chloride, possibly for sulfate at longer times
- High chloride contents are found in the pits and in corrosion products, especially in the vicinity of the interface: formation of Cl-rich phases in the 52-month test.
- The sequence of formation of corrosion products, under unsaturated conditions and low RH% values, begins with the precipitation of Fe(OH)₃ and lepidocrocite followed by goethite. The end-products of this transformation are anhydrous oxides (hematite, maghemite and finally magnetite).
- Chloride, due to its hygroscopicity, initializes electrochemical corrosion at low RH (~50%).
- In general, in the tests dismantled, corrosion is scarce and localized, especially in Cl-rich areas on the bentonite surface.

- Under reducing conditions and RH% close to 50% (52-month test), corrosion products layer coating the Fe particles was hardly few tens of nanometers-thick, despite high reactivity of particulate iron.
- Formation of Cl-rich phases is possible: akaganeite was identified at the bottom of the pits in the steel plate test and in the 52-month test.

7. REFERENCES

- [1] M.J. Turrero, Deliverable D2.3-3-1: Laboratory tests at the interfaces. First results on the dismantling of tests FB3 and HB4, Ciemat, Madrid, 2011.
- [2] E. Torres, J. Peña, M.J. Turrero, P.L. Martín, A. Escribano, M.V. Villar, Different stages on the corrosion phenomena during the lifetime of a Deep Geological Repository, in: D. Féron (Ed.), Eurocorr 2008, European Federation of Corrosion Edimburgh, UK, 2008.
- [3] E. Torres, A. Escribano, J.L. Baldonado, M.J. Turrero, P.L. Martín, J. Peña, M.V. Villar, Evolution of the geochemical conditions in the bentonite barrier and its influence on the corrosion of the carbon steel canister, Materials Research Society, Warringdale, PA, 2009.
- [4] E. Torres, Geochemical processes at the C-steel/bentonite interface in a Deep Geological Repository: experimental approach and modeling, Ciencia de los Materiales e Ingeniería Metalúrgica, Universidad Complutense de Madrid, Madrid, 2011, p. 450.
- [5] L. Johnson, F. King, The effect of the evolution of environmental conditions on the corrosion evolutionary path in a repository for spent fuel and high-level waste in Opalinus Clay, J. Nucl. Mat. 379 (2008) 9-15.
- [6] ENRESA, Evaluación del comportamiento y de la seguridad de un almacenamiento geológico profundo en granito, Publicación técnica 6/97, ENRESA, Madrid, 1997, p. 179.
- [7] F.J. Samper, L. Montenegro, Time evolution of temperatures at the canister and bentonite-granite interface, La Coruña, 2010.
- [8] F. King, Evolution of environmental conditions in a deep geological repository in the sedimentary rocks of the Michigan Basin, Ontario Power Generation. , 2005.
- [9] G.A. Henshall, Numerical Predictions of Dry Oxidation of Iron and Low-Carbon Steel at Moderately Elevated Temperatures, in: T. Abrajano (Ed.), Scientific Basis for Nuclear Waste Management XIV, Materials Research Society, Pittsburgh, PA, 1996.
- [10] J.C. Estill, G.E. Gdowski, The effect of water vapor on the corrosion of carbon steel at 65°C, in: H.A. Dockery (Ed.), Seventh International Conference on High Level Radioactive Waste Management, ASCE, New York, 1996.

- [11] D. Stahl, J.K. McCoy, Impact of Thermal Loading on Waste Package Material Performance, in: T. Murakami, R.C. Ewing (Eds.), *Scientific Basis for Nuclear Waste Management XVIII*, Materials Research Society, Pittsburgh, PA, 1995.
- [12] J.K. McCoy, Updated Report on RIP/YMIM Analysis of Designs, Yucca Mountain Site Characterization by TRW Environmental Safety Systems, DOE, 1995.
- [13] N. Birks, G.H. Meier, *Introduction to High Temperature Oxidation of Metals*, Edward Arnold, London, 1983.
- [14] D. Caplan, M. Cohen, Effect of cold work on the oxidation of iron from 400-650°C, *Corros. Sci.* 6 (1966) 321-335.
- [15] A. Terlain, D. Desranges, D. Gauvain, D. Féron, P. Galtayries, *CORROSION/2001*, NACE International Houston, TX 2001, p. Paper No. 01119 02001.
- [16] S. Ben Lagha, D. Crusset, I. Mabile, M. Tran, M.C. Bernard, E. Sutter, Corrosion of iron: A study for radioactive waste canisters, *J. Nucl. Mat.* 362 (2007) 485-492.
- [17] M. Tullmin, P.R. Roberge, in: W. Revie (Ed.), *Uhlig's Corrosion Handbook*, John Wiley, New York, 2000, p. 309.
- [18] J.F. Dante, R.G. Kelly, The evolution of the adsorbed solution layer during atmospheric corrosion and its effects on the corrosion rate of copper, *J. Electrochem. Soc.* 140 (1993) 1890-1897.
- [19] S. Lee, S. R.W, Adsorption of Water on Copper, Nickel and Iron, *Corrosion* 53 (1997) 33-42.
- [20] V. Kucera, E. Mattson, *Atmospheric Corrosion* in: F. Mansfeld (Ed.), *Corrosion Mechanisms*, Marcel Dekker, Inc., New York, 1987, pp. 211-252.
- [21] E.W. Washburn, *International Critical Tables of Numerical Data, Physics, Chemistry and Technology*, McGraw-Hill Book Company, Inc, New York, 1928.
- [22] T.E. Graedel, R.P. Frankental, Corrosion mechanisms for iron and low-alloy steels exposed to the atmosphere, *J. Electrochem. Soc.* 137 (1990) 2385-2394.
- [23] G.E. Gdowski, Humid Air Corrosion of YMP Waste Package Candidate Material, *CORROSION NACExpo 98*, San Diego, 1998.
- [24] A.R. Hoch, K.A. Cliffe, B.T. Rodwell, Modelling gas migration in compacted bentonite: GAMBIT club phase 3. Final Report. , POSIVA Oy, 2004.
- [25] W.R. Rodwell, A.W. Harris, S.T. Horseman, P. Lalieux, W. Müller, L. Ortiz Amaya, K. Pruess, Gas Migration and Two-Phase Flow through Engineered and Geological Barriers for a Deep Repository for Radioactive Waste, in: E. Commission (Ed.), *Nuclear Science and Technology*, European Commission, Brussels, 1999.

- [26] C.C. Naish, P.H. Balkwill, T.M. O'brien, K.J. Taylor, G.P. Marsh, The Anaerobic Corrosion of Carbon steel in Concrete, in: E. Commission (Ed.), Nuclear Science and Technology, European Commission, Brussels, 1991.
- [27] P.J. Agg, Modelling Gas Generation in Radioactive Waste Repositories, Nuclear energy 32 (1993) 81-87.
- [28] N. Platts, D.J. Blackwood, C.C. Naish, Anaerobic Oxidation of Carbon Steel in Granitic Groundwaters: A review of relevant literature, in: SKB (Ed.), Technical Report, SKB, Stockolm, Sweden, 1994.
- [29] N.R. Smart, D.J. Blackwood, L. Werme, Anaerobic Corrosion of Carbon Steel and Cast Iron in Artificial Groundwaters: Part 1 - Electrochemical Aspects, Corrosion 58 (2002) 547-559.
- [30] V.J. Linnenbom, The reaction between iron and water in the absence of oxygen, J. Electrochem. Soc. 105 (1958) 322-324.
- [31] N.R. Smart, D.J. Blackwood, L. Werme, Anaerobic Corrosion of Carbon Steel and Cast Iron in Artificial Groundwaters: Part 2 - Gas Generation, Corrosion 58 (2002) 627-637.
- [32] B. Kurten, E. Smailos, I. Azkarate, L. Werme, N.R. Smart, G. Santarini, COBECOMA, State-of-the-art Document on the COrrOsion BEhaviour of COntainer Materials, in: E. Commission (Ed.), European Commission, Brussels, 2004, p. 299.
- [33] ENRESA, Chemical (thermo-hydromechanical) evolution of the EBS: evolution of porewater chemistry; effects of canister corrosion and concrete degradation; and radionuclide retention. NF-PRO project., in: Enresa (Ed.), Enresa, Documentos internos de referencia Madrid 2008.
- [34] ENRESA, FEBEX Project Final Report. Post-mortem bentonite analysis, Publicación Técnica, ENRESA, Madrid, 2006b, p. 183.
- [35] J. Cuevas, M.V. Villar, A.M. Fernández, P. Gómez, P.L. Martín, Pore waters extracted from compacted bentonite subjected to simultaneous heating and hydration, Appl. Geochem. 12 (1997) 473-481.
- [36] J. Cuevas, M.V. Villar, M. Martín, J.C. Cobeña, S. Leguey, Thermo-hydraulic gradients on bentonite: distribution of soluble salts, microstructure and modification of the hydraulic and mechanical behaviour, Appl. Clay Sci. 22 (2002) 25-38.
- [37] J.I. Drever, The Geochemistry of Natural Waters, Prentice Hall, New Jersey, 1988.
- [38] A.M. Fernández, M.V. Villar, Geochemical behaviour of bentonite barrier: results up to 8 years of thermo-hydraulic treatment in the laboratory, Ciemat, Madrid, 2008.
- [39] J. Majzlan, K.-D. Grevel, a. Navrotsky, Thermodynamics of Fe oxides: Part II. Enthalpies of formation and relative stability of goethite (α -FeOOH), lepidocrocite (γ -FeOOH) and maghemite (γ -Fe₂O₃), Am. Mineral. 88 (2003) 855-859.

Appendix - Geochemical data

Soluble anions

Table A- 1. Soluble chloride in the medium cells dismantled.

6 months		15 months		52 months	
Distance from hydration (mm)	Chloride (mmol/100 g)	Distance from hydration (mm)	Chloride (mmol/100 g)	Distance from hydration (mm)	Chloride (mmol/100 g)
14	0,43	14	0,11	12	0,01
42	4,2	42	0,28	32	0,02
71	4,27	71	5,77	47	0,01
86	0,06	86	11,94	57	0,01
Fe powder	0	Fe powder	0	75	5,06
FEBEX Bentonite – reference value: 1.8 mmol/100 g				Fe powder	1,44

Table A- 2. Soluble sulfate in the medium cells dismantled.

6 months		15 months		52 months	
Distance from hydration (mm)	Sulfate (mmol/100 g)	Distance from hydration (mm)	Sulfate (mmol/100 g)	Distance from hydration (mm)	Sulfate (mmol/100 g)
14	0,02	14	0,06	12	0,01
42	0,80	42	1,79	32	0,04
71	0,39	71	0,96	47	0,86
86	1,69	86	0,87	57	0,26
Fe powder	0	Fe powder	0	75	1,58
FEBEX Bentonite – reference value: 0.71 mmol/100 g				Fe powder	$7 \cdot 10^{-3}$

Soluble cations

Table A- 3. Soluble sodium in the medium cells dismantled.

6 months		15 months		52 months	
Distance from hydration (mm)	Sodium (mmol/100 g)	Distance from hydration (mm)	Sodium (mmol/100 g)	Distance from hydration (mm)	Sodium (mmol/100 g)
14	3,5	14	3,3	12	2,5
42	5,9	42	5,3	32	2,2
71	6,9	71	8,5	47	3,4
86	8,59	86	10,8	57	2,4
FEBEX Bentonite – reference value: 6,5 mmol/100g				75	7,9

Table A- 4. Soluble potassium in the medium cells dismantled.

6 months		15 months		52 months	
Distance from hydration (mm)	Potassium (mmol/100 g)	Distance from hydration (mm)	Potassium (mmol/100 g)	Distance from hydration (mm)	Potassium (mmol/100 g)
14	0,18	14	0,26	12	0,03
42	0,09	42	0,04	32	0,02
71	0,03	71	0,18	47	0,04
86	0,10	86	0,26	57	0,02
FEBEX Bentonite – reference value: 0,06 mmol/100g				75	0,31

Table A- 5. Soluble calcium in the medium cells dismantled.

6 months		15 months		52 months	
Distance from hydration (mm)	Calcium (mmol/100 g)	Distance from hydration (mm)	Calcium (mmol/100 g)	Distance from hydration (mm)	Calcium (mmol/100 g)
14	0,13	14	0,22	12	0,03
42	0,22	42	0,29	32	0,01
71	0,02	71	0,46	47	0,03
86	0,30	86	0,40	57	0,03
FEBEX Bentonite – reference value: 0,07 mmol/100g				75	0,29

Table A- 6. Soluble magnesium in the medium cells dismantled.

6 months		15 months		52 months	
Distance from hydration (mm)	Magnesium (mmol/100 g)	Distance from hydration (mm)	Magnesium (mmol/100 g)	Distance from hydration (mm)	Magnesium (mmol/100 g)
14	0,05	14	0,02	12	0,04
42	0,11	42	0,14	32	0,01
71	0,14	71	0,44	47	0,01
86	0,07	86	0,36	57	0,01
FEBEX Bentonite – reference value: 0,06 mmol/100g				75	0,49

Exchangeable cations

Table A- 7. Average values for exchangeable cations in FEBEX bentonite

FEBEX	Na (meq/100 g)	K (meq/100 g)	Mg (meq/100 g)	Ca (meq/100 g)
Reference values	27	3	31	35

Table A- 8. Exchangeable cations for the 6-month medium-cell experiment

Distance from hydration (mm)	Na (meq/100 g)	K (meq/100 g)	Mg (meq/100 g)	Ca (meq/100 g)
14	35	3	27	35
42	34	3	27	36
71	26	3	36	35

Table A- 9. Exchangeable cations for the 15-month medium-cell experiment

Distance from hydration (mm)	Na (meq/100 g)	K (meq/100 g)	Mg (meq/100 g)	Ca (meq/100 g)
14	38	3	20	38
42	35	3	27	35
71	28	3	34	35

Table A- 10. Exchangeable cations for the 52-month medium-cell experiment

Distance from hydration (mm)	Na (meq/100 g)	K (meq/100 g)	Mg (meq/100 g)	Ca (meq/100 g)
12	31	2	21	40
32	29	2	20	41
47	27	2	20	40
57	28	1,5	21	42
75	15	3	44	26